JOURNAL OF MATERIALS SCIENCE 9 (1974) 1507–1516

The structure and mechanical properties of polyoxymethylene polymerized in the solid state

E. H. ANDREWS, G. E. MARTIN*
Department of Materials, Queen Mary College, University of London, UK

Polyoxymethylene specimens with single crystal texture were produced by irradiation of needle-shaped trioxane crystals subsequently post-polymerized at fixed temperatures between 30 and 60° C. A clear dependence of polymer conversion on irradiation dose and polymerization temperature was revealed. The polymer morphology consisted of mutually aligned fibrils, half of which were chain-extended crystallites with their molecular axes coincident with the specimen axis. The remaining fibrils consisted of folded chains in a "twin" configuration.

The degree of order in the specimens was analysed in terms of the arcing of X-ray diffraction spots. There existed an intrinsic level of misorientation of molecules which depended on the post-polymerization temperature, plus a misalignment due to displacement of fibrils on the removal of unreacted monomer. Finally, the mechanical properties were investigated and the Young's modulus was found to approach closely its theoretical limit at the conversion maximum. The results are interpreted on the basis of a simple morphological model.

1. Introduction

In recent years much effort has been applied to obtaining molecular extension and alignment in solid polymers with the aim of exploiting the high strength and stiffness of the covalently bonded backbone. Fully extended and aligned long chain polymers would have a Young's modulus in the alignment direction similar to that of steel, but even with a high degree of molecular alignment, commercially available polymers fall far short of their theoretically attainable moduli. This, of course, is due to the predominance of chain folding in polymer crystals. The "elastic" compliance of such materials is not governed by the stretching of extended chains, as in an idealized morphology, but results from a combination of deformation modes including deformation of the softer intercrystalline regions and anelastic deformations in the chain-folded lamellae themselves. Solid state polymerization offers one method of obtaining extended-chain crystal morphologies which should be capable of near-ideal elastic moduli.

In this study we have investigated the variations in properties and structure which occur in a solid-state polymerized material as a result of differences in specimen preparation. The preparation technique employed was the radiation-induced solid state polymerization of single crystals of trioxane to highly oriented specimens of fibrous polyoxymethylene. This polymerization system was selected to obtain polymer specimens with morphologies close to the ideal situation of fully extended and aligned molecules. The mechanical properties in the direction of molecular alignment have been measured and the results correlated with the polymer structure.

In their study of the post-polymerization of irradiated trioxane, Hayashi *et al.* [1] found that a saturation yield was reached, and that both saturation yield and initial polymerization rate increased on increasing the irradiation dose. They also showed that these quantities were affected by the crystalline state of the monomer, in that large monomer crystals could be polymerized to higher conversions than aggregates of small crystals. In the same work, the authors attempted to elucidate the mechanism of post-polymeriza-

*Present address: The Corporate Laboratory, ICI Ltd, Runcorn, Cheshire.

tion in trioxane. Because of the high activation energy of the process, they ruled out the possibility of an ionic mechanism and from electron spin resonance measurements it appeared unlikely that a radical mechanism was involved. However, it was found that the behaviour of peroxides present in the irradiated monomer followed that of the polymerization reaction and also that rapid decomposition of the peroxides occurred at temperatures corresponding to the onset of post-polymerization. Furthermore, the energy of formation of the peroxides is of the same order as the overall activation energy of polymerization. The authors concluded that the post-polymerization of trioxane depends on an active species originating from the decomposition of peroxides and not from an ionic or trapped radical mechanism.

The crystal structure of this material has been the subject of some debate in the literature [2-6]. A previous paper [7] was concerned with the study of this problem by X-ray diffraction and led to the conclusion that helical molecular configurations such as that of polyoxymethylene are best described in terms of the parameters which define a helix, plus the symmetry and separation of the chains.

An interesting feature of the polyoxymethylene produced by solid state polymerization of trioxane is that it co-exists in two crystalline modifications. The "main" orientation has the molecular axis aligned with the monomer crystal *c*-axis, whilst in the "twin" orientation an angle of 76° lies between the molecular axis and the parent crystal *c*-axis. Each modification was found [8] to be present in approximately equal abundance. Colson and Reneker [9, 10] observed that both the "main" and the "twin" orientations grow into long, slender fibrils all of which are mutually aligned. They deduce that in "main" orientation fibrils the molecules are extended and aligned with the fibril axis and that in "twin" orientation fibrils the molecules are back-folded.

Small-angle X-ray diffraction studies [11, 12] revealed no peak in the scattering from the material obtained by the polymerization of trioxane in the solid state, suggesting [13] that the product was solely polyoxymethylene with aligned and extended molecules. However, the chain-folded configurations are not detected by low-angle diffraction because the fold length in a single specimen can assume a wide range of values between 10 nm and 1 μm [14].

Sakurada *et al.* [15] determined the Young's modulus of the crystalline regions in a highly drawn sample of commercial polyoxymethylene (Delrin) using X-ray diffraction to measure the lattice extension under constant stress applied in the direction of the chain axis. They arrived at a value of 5.34×10^{10} N m^{-2} which is in good agreement with the value of 4.1×10^{10} N m^{-2} calculated by Miyazawa [16] for the polyoxymethylene helix in its hexagonal crystalline configuration. The tensile strength of narrow, thread-like crystals of polyoxymethylene obtained by polymerization of trioxane was measured by Slutsker *et al.* [17] who found failure stresses in the range (0.36 to 3.6) $\times 10^9$ N m^{-2}.

2. Specimen preparation

Since it was known [1] that the state of the parent crystal can play an important role in its polymerization, care was taken to ensure that the trioxane crystals were as nearly identical as possible. The crystals were grown by sublimation in closed and carefully cleaned containers exposed to a slight temperature gradient over their volume. The presence of small quantities of water could inhibit the post-polymerization of irradiated trioxane [1], and some phosphorus pentoxide was therefore placed in each vessel to obtain an equally dry set of monomer crystals. Trioxane single crystals of approximately equal width were collected from the growth vessels and each was cut to the same length. The specimens were needle shaped with a width of approximately 1 mm and length of 45 mm. They were sealed in air in clean glass tubes where they remained until the post-polymerization was completed. An air atmosphere has been shown [18] to increase both the rate of polymerization and the ultimate degree of conversion.

The specimens, in groups of five, were irradiated with high-energy electrons to a number of doses in the range 0.01 to 10.0 Mrad, each group later contributing one specimen to each of five constant temperature baths set at 30, 40, 50, 55 and 60°C. The irradiation was carried out on the 15 MeV linear electron accelerator at St. Bartholomew's Hospital, London. Throughout irradiation and afterwards, until immersion in the post-polymerization baths, the samples were maintained at − 76°C. Post-polymerization was carried out for 48 h, the period being chosen to ensure that the reaction would be completed at the lower temperatures where the polymerization

proceeds more slowly [18]. After post-polymerization the unconverted monomer was extracted by washing in acetone and drying under vacuum for a further 48 h.

3. Characterization of the conversion

The principal distinction between specimens polymerized under differing conditions is their ultimate degree of conversion. After the residual polymer had been isolated, it was weighed and the percentage conversion determined from the expression:

$$\text{conversion} = 100 \times \frac{\text{weight of residual polymer}}{\text{weight of initial monomer}} \%.$$

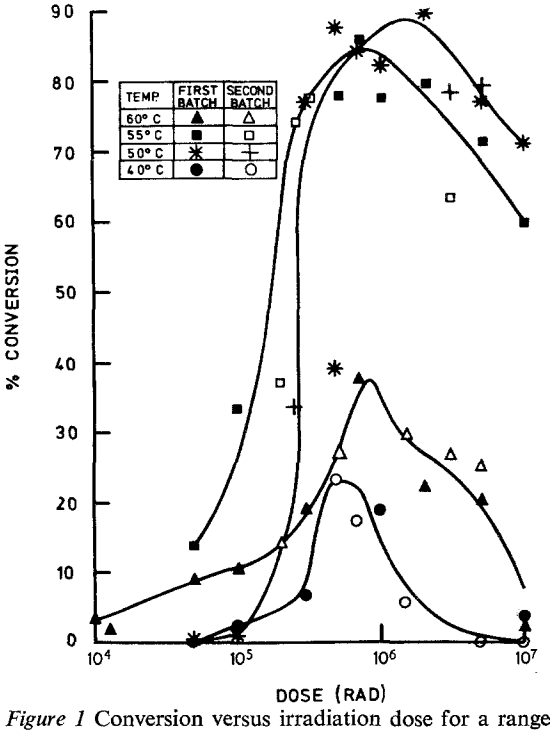

Figure 1 Conversion versus irradiation dose for a range of post-polymerization temperatures.

The results are shown in Fig. 1 where the percentage conversion is plotted against the logarithm of irradiation dose for each temperature of post-polymerization. No polymer was formed, for any dose, at 30°C. The empty and filled symbols in Fig. 1 denote results obtained from separate growth and polymerization batches, thus demonstrating the reproducibility of the data. In each of the curves of Fig. 1 there is a clear maximum in the conversion in the dose range 0.5 to 2.0 Mrad. The gradients of the curves on the low dose side of the maxima are much greater than those on the high dose side and the latter parts of the plots are approximately parallel. This indicated that the rate of decrease in conversion is independent of polymerization temperature.

These observations are compatible with the following scheme. Irradiation implants in the monomer crystal active species which initiate polymerization to an extent dependent upon the density of such species and the post-polymerization temperature (which causes rising molecular activity as it is raised). However, as the monomer melting point of 62°C is approached, the accompanying reduction of order in the trioxane crystal inhibits the polymerization mechanism and the conversion falls. Also at irradiation doses above the optimum, the conversion decreases (at a rate independent of the polymerization temperature) due to the effect of radiation damage to the monomer crystal or to "poisoning" by radiolysis products which increase in abundance with dose.

4. Characterization of the structure

4.1. Arcing of X-ray reflections

The resulting polyoxymethylene has a morphology of mutually aligned fibrils. An estimate of the dimensions of the fibrils (0.5 μm width by 50 μm length) was obtained from optical microscopy of fibrils dispersed in water by ultrasonic vibrations.

In such a morphology a property of importance is the degree of molecular alignment which the specimens possess. We have studied this aspect of the structure by measuring the arcing of the "main" X-ray reflections which occurs as a result of misaligned molecular *c*-axes.

Rotation X-ray diffraction photographs were taken of each polymer specimen, the rotation axis being the axis of the specimen which coincides with the direction of the "main" crystal *c*-axis. Nickel filtered copper radiation was used and the camera diameter was 57.3 mm. As the X-ray beam was normal to the rotation axis, the equatorial reflections were from planes parallel to the "main" crystal molecular axis. It was very noticeable that the diffraction patterns of specimens polymerized at higher temperatures were generally more arced and diffuse than of those polymerized at lower temperatures.

Quantitative data were obtained by scanning on a microdensitometer the (110), (200) and

(210) reflections along their arc lengths. The lines of arcing due to the misorientation of x-axes about the rotation axis are those of constant lattice spacing; i.e. the intersection of spheres with the cylindrical film. For convenience, the reflections were scanned in a direction perpendicular to the equator. This is a perfectly adequate method for relatively sharp spots but it introduces some error in the measurements of more heavily arced reflections.

The arc lengths were compared by measuring the width at half intensity of each microdensitometer scan. These widths are dependent upon the Bragg angle, θ, and the mean angle, Δ, of apparent c-axis misorientation in the specimen (The true angle of c-axis misorientation, ψ, is obtained by correcting for beam divergence; see below). Allowance was made for these dependences and the widths were converted into their related Δ by means of a calibration obtained from the appropriate ρ, θ, ϕ chart. (The charts, which are designed as an aid to interpretation of "tilted-crystal" diffraction patterns, are obtainable from the Institute of Physics.)

From the geometry of the X-ray collimator and its position in relation to the specimen and the camera, the spot width, δ, due to beam divergence was calculated. The widths due to arcing and divergence were separated by the Scherrer Approximation [19], i.e. the mean angle of c-axis misorientation is given simply by $\psi \equiv (\Delta\text{-}\delta)$. The results are shown in Fig. 2, where the

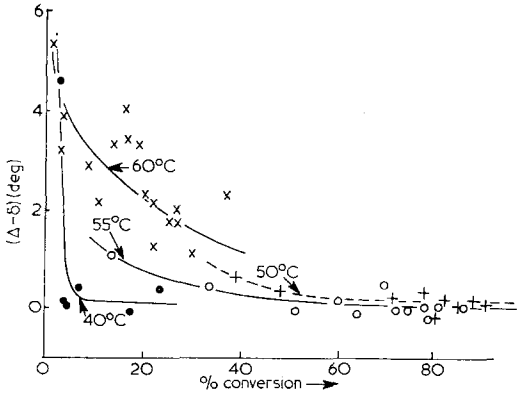

Figure 2 c-axis misorientation versus conversion.

mean angle of misorientation is plotted against conversion for the four temperatures of post-polymerization. The values for each specimen are the average of the figures yielded from the separate X-ray reflections. It is noticeable that there is a considerable scatter in the 60°C results and this presumably is due to the error introduced by scanning along straight lines.

The curve obtained for post-polymerization at 40°C is striking. It displays a very high degree of molecular alignment until the conversion becomes very low, at which point the specimens become highly disordered. The 60°C results, in contrast, exhibit overall disorder which gradually increases as conversion falls. The 50 and 55°C curves lie between those for 40 and 60°C but no data for very low conversions were available. These trends appear to be independent of whether the low conversions arise from doses smaller or larger than the maxima in Fig. 1.

It is to be expected that, in polymer formed at temperatures close to the monomer melting point, the overall degree of disorder would be somewhat greater than in material polymerized at lower temperatures.

A possible explanation of increasing misorientation with decreasing conversion is that the fibrils tilt or bend as the unconverted monomer is removed. The lower the conversion, the larger are the voids through which the polymer fibrils can move.

4.2. Critical test

An experiment was conducted to test the hypothesis proposed above. Trioxane crystals were grown, irradiated and post-polymerized at 40 and 60°C, these being the two extreme temperatures where large misorientations were observed at sufficiently low conversion. Irradiation doses of 10 and 100 Krad for the 60 and 40°C specimens respectively were delivered in order to attain conversions appropriate for large c-axis misorientation (see Fig. 1). Rotation X-ray diffraction photographs were taken of each specimen whilst they were sealed in glass capillaries so that the unreacted monomer was still present and could not sublime. After exposure, the monomer was carefully pumped away and further diffraction patterns were taken of the polymer alone. Finally the conversion of each specimen was determined.

The results of the 40°C post-polymerization are illustrated in Fig. 3a and b and those of the 60°C case are shown in Fig. 4a and b. Both figures exhibit the rotation X-ray diffraction photographs taken before and after removal of the unconverted monomer respectively. Fig. 3a shows clear and sharp reflections for both the

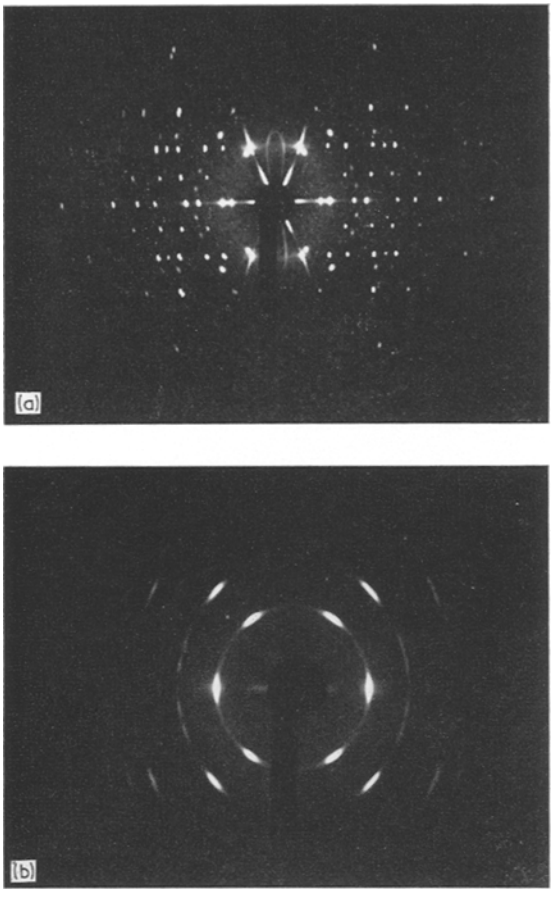

Figure 3 Rotation X-ray diffraction pattern of (a) specimen polymerized at 40°C, and (b) same specimen after removal of monomer.

trioxane and polyoxymethylene lattices. The broadening of some of the polyoxymethylene equatorial reflections were scanned on the microdensitometer and were found to be approximately equivalent to the spot width due to beam divergence. On removal of the monomer the polymer pattern became broadly arced as can be seen in Fig. 3b. The broadening was measured and it was found to correspond to a *c*-axis misorientation of approximately 4°. The conversion of this specimen was 4% and so the result agrees precisely with the findings displayed in Fig. 2.

The pattern of the specimen polymerized at 60°C (see Fig. 4a) again showed reflections for both monomer and polymer lattices, but in this case the polyoxymethylene spots were more arced than those of trioxane. Measurements of the polymer equatorial reflections indicated that there was an intrinsic *c*-axis misalignment within the fibrils of about 1°. The arcing of the polymer reflections was found to have increased considerably on removal of unreacted trioxane (see Fig. 4b) and the broadening measurements here yielded a *c*-axis misorientation of nearly 6°. These findings also agree well with initial experimental results. The results of these critical tests show conclusively that apart from some small intrinsic misorientation at the higher polymerization temperatures, the *c*-axis misalignment derives from the buckling of fibrils when residual monomer is removed.

5. Mechanical properties

5.1. Experimental procedure

The Young's modulus of the polyoxymethylene needles was measured with the aid of the extensometer rig shown schematically in Fig. 5.

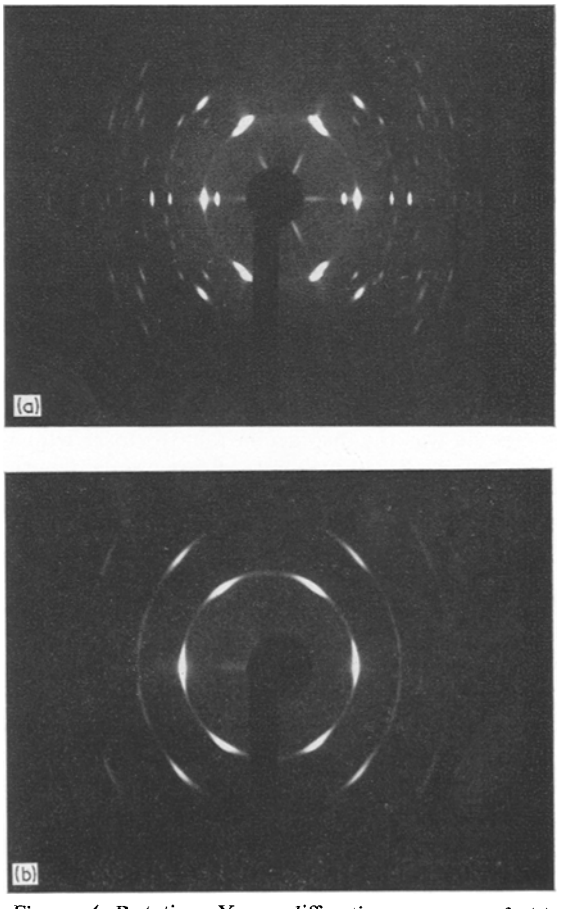

Figure 4 Rotation X-ray diffraction pattern of (a) specimen polymerized at 60°C, and (b) same specimen after removal of monomer.

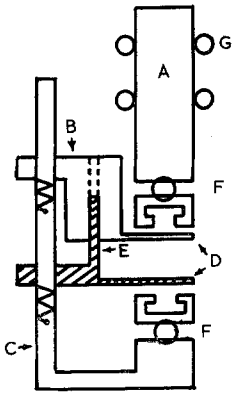

Figure 5 Schematic representation of extensometer rig: A = shaft connected to load cell and cross-head, B = transducer, C = support rods, D = gauge-length arms, E = armature, F = universal joints, G = PTFE bushes.

The rig, which was constructed specifically for this purpose, was operated as an attachment to an Instron machine. Specimens were set (using epoxy resin) in stainless steel end-blocks and gauge-length discs whilst held in an adjustable rig to ensure axial placement. Fig. 6 is a schematic representation of a specimen prepared for

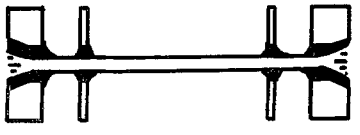

Figure 6 Section through specimen prepared for test.

testing. The principal component of the extensometer rig was the displacement transducer which monitored the movement of the gauge-length discs by means of the counter-balanced arms. The transducer output was demodulated, amplified and filtered before being fed into the "X" channel of an X-Y recorder. The "Y" channel was fed from the Instron load cell amplifier. After careful calibration of the transducer system, the performance of the instrumentation was thoroughly tested and proved with the use of dummy specimens turned in mild steel.

Before measurements were carried out on the same carefully prepared specimens, which had been subjected to the structural investigations, experience was gained in handling the samples by performing initial tests on less well characterized material. Load-extension curves were plotted, both in loading and unloading at three rates of extension (0.1, 0.2 and 0.4 mm min^{-1}). Finally,

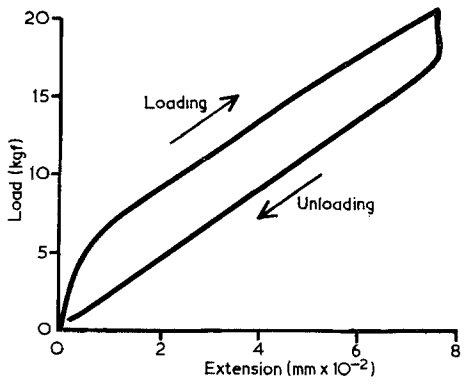

Figure 7 Plot of load versus extension.

the specimens were extended until failure. A typical load-extension plot is shown in Fig. 7. The initial steep region of the plot and the steep part immediately after reversing the cross-head motion are due to the taking up of a small amount of bending in the gauge-length arms, and are ignored in calculating the Young's modulus. The modulus results are the mean of six independent measurements, i.e. loading and unloading at three rates of extension. The average cross-sectional area of each specimen was calculated from the weight, length and density of the parent monomer crystal. This yielded the area associated with the outer dimensions of the sample, since it was observed that the dimensions remained unaltered during polymerization. The Young's moduli were, therefore, measurements for the bulk specimen making no allowance for the fact that lower conversions result in fewer fibrils per unit cross-sectional area than higher conversions.

5.2. Results

The Young's moduli for all specimens are shown plotted against their conversions in Fig. 8, where the broken line represents theoretical behaviour, i.e. the modulus which would be recorded for needles composed of load-bearing elements, with theoretical modulus, extending in parallel over the entire length of the specimen. The failure stress recorded for each sample is shown against its mean Young's modulus in Fig. 9. The best line through the points has a gradient of 0.06 but the upper-bound line has a slope of 0.1, very close to a theoretical value for the ratio of breaking stress to modulus.

From Fig. 8 it is clear that the "gradient" of an experimental point, namely the Young's

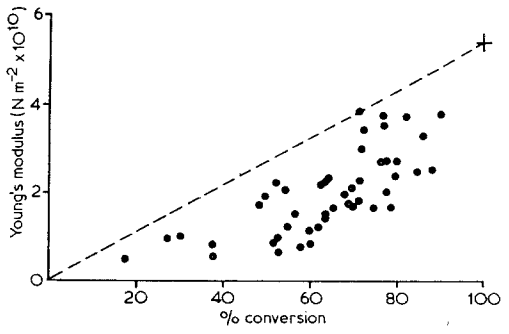

Figure 8 Young's modulus versus conversion.

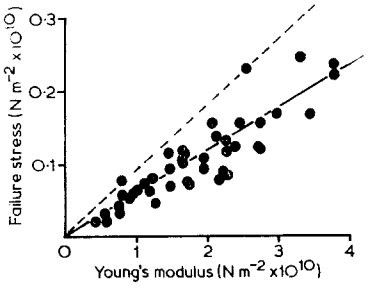

Figure 9 Failure stress versus Young's modulus.

modulus, E, divided by conversion fraction, β, is a measure of the closeness of the result to theoretical behaviour. Fig. 10 is a plot of the quantity E/β against irradiation dose for well characterized specimens only. Results for samples polymerized at the same temperatures are represented by identical symbols and the broken lines are the envelope of the data. The tendency towards theoretical modulus is clearly optimized at a dose of around 1.0 Mrad. Although this plot eliminates the simple effect of conversion, (i.e. increasing conversion increases the number of load-bearing elements per unit cross-sectional area) the results exhibit a close similarity to the conversion versus dose curves of Fig. 1, and the envelope of the data points is drawn in Fig. 10 to emphasize this. In spite of this similarity, however, attempts to correlate E/β with conversion β directly are *not* successful.

Below is proposed a "composite" model which accounts for these effects in a semi-quantitative manner and which has the virtue of being physically realistic.

5.3. Adhesive-fibril model for solid-state polymerized POM

Consider the volume of the original trioxane

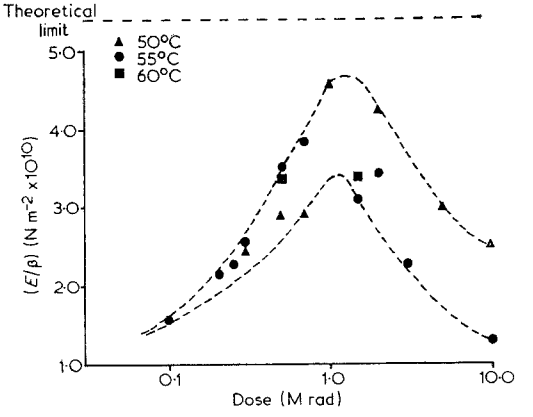

Figure 10 Young's modulus/conversion versus dose.

crystal lattice to be divided into cubic segments of cube-edge d, and suppose that conversion to polymer results in a volume fraction β of the material being converted into polymer in the form of fibrils of width d, breadth d, and length nd, where $2n$ is the aspect ratio. The fibrils grow with a common orientation (Fig. 11).

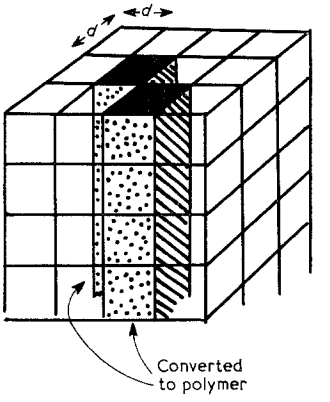

Figure 11 Model fibrillar structure.

Consider an element of the "d-lattice". The probability that it is occupied by polymer is, of course, β, and the probability that an immediately adjacent cell (in a plane perpendicular to the fibril length is *also* occupied by polymer is β^2. The total side surface area of a fibril is,

$$A = 4nd^2 \qquad (1)$$

so that the total area of side-contact is given by

$$\beta^2 A = 4nd^2\beta^2 . \qquad (2)$$

The longitudinal tensile stress, σ_f, in a fibril is

transferred to other fibrils only through these side contacts, the interfacial material being in shear. If G_i is the shear modulus of the interface, and the total load, $\sigma_f d^2$, on a given fibril is carried evenly by the interfacial contact regions, the interfacial strain becomes

$$\gamma_i = \frac{\sigma_f d^2}{4nd^2\beta^2}\frac{1}{G_i} = \frac{\sigma_f}{4n\beta^2 G_i} . \quad (3)$$

The total contribution, ϵ_i, of this shear strain to the tensile strain of the specimen is not easy to assess, since it depends upon the exact morphology of the specimen and the thickness, h, of the interface. The morphological factor can best be illustrated by Fig. 12. Fig. 12a shows a

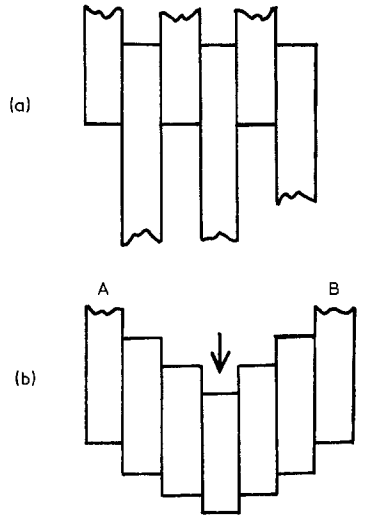

Figure 12 (a) Interleaved fibrils (schematic). (b) "Accordian" fibril structure (schematic).

closely packed array of fibrils which interleave, and the contribution of inter-fibrillar shear to tensile strain is of the order of

$$\epsilon_i \simeq \gamma_i h/nd \quad (4)$$

nd being the length of a fibril. By contrast the more open "accordian" type structure of Fig. 12b can contribute a maximum strain

$$\epsilon_i \simeq \gamma_i hN/2nd \quad (5)$$

where N is the number of fibrils between "fixed points" A and B. Fortunately, all possibilities can be approximated by realising that N will have an average value given by

$$N = (1 - \beta)/\beta \quad (6)$$

so that

$$\epsilon_i = (1 - \beta)\gamma_i h/2nd\beta . \quad (7)$$

The strain in the fibril itself is, of course,

$$\epsilon_f = \sigma_f/E_0 \quad (8)$$

where E_0 is the Young's modulus of the fibril, and the total strain will, therefore, be

$$\epsilon = \epsilon_i + \epsilon_f = \sigma_f\left[\frac{1}{E_0} + \frac{h(1-\beta)}{4n^2 d\beta^3 G_i}\right] . \quad (9)$$

The specimen modulus is then

$$E = \beta\sigma_f/\epsilon = \beta\left[\frac{1}{E_0} + \frac{h(1-\beta)}{4n^2 d\beta^3 G_i}\right]^{-1} \quad (10)$$

or

$$\frac{E}{\beta E_0} = \left[1 + \frac{E_0}{G_i}\frac{h}{d}\frac{(1-\beta)}{4n^2\beta^3}\right]^{-1} . \quad (11)$$

Unfortunately, it is not possible to evaluate the RHS of this equation with any great confidence, since G_i, and (h/d) are not known. However, if plausible values are taken, E_0/G_i may be of the order of 10^3 and (h/d) of the order of 0.1, giving

$$\frac{E}{\beta E_0} \simeq \left\{1 + \frac{100(1-\beta)}{(2n)^2\beta^3}\right\}^{-1} . \quad (12)$$

The LHS of this equation being the fraction of theoretical modulus attained for any given degree of conversion β.

The RHS of Equation 12 is plotted against β in Fig. 13 for various choices of the fibril aspect ratio $(2n)$, together with experimental points. The experimental data for 50 and 55°C fit extremely well the theoretical curve for an aspect ratio of 6, although the low-dose specimens polymerized at 55°C are better described by an aspect ratio of 20. The limited data for 60°C agree well with an aspect ratio of 55. It must be emphasized that the aspect ratio values for best fit are governed by the choices of E_0/G_i and of h both of which can only be guessed. The facts remain that the *form* of dependence upon β of the modulus is very well predicted by the theory, and that the aspect ratio values required to fit the data are not wildly unrealistic. There is the further implication that the aspect ratio of the polymer fibrils is dependent upon the conditions of irradiation and polymerization.

6. Structure-property relationships

The previous section shows that the modulus data can be rationalized in terms of a "composite" model provided that the aspect ratio of the fibrils depends upon the temperature of poly-

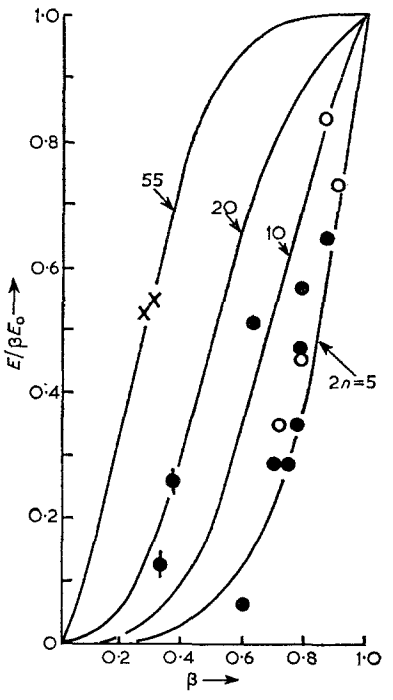

Figure 13 Fraction of theoretical modulus achieved, as a function of conversion, β. Points are experimental data: (○) polymerized at 50°C; (●) at 55°C; (◐) at 55°C after low irradiation doses; (×) at 60°C. Lines show theory for various aspect ratios, 2n, as indicated.

merization and, to a lesser extent, upon the irradiation dose. The limited data at 55°C suggest that at a given temperature the aspect ratio increases as the dose decreases. This might be expected since fewer initiation sites must give rise to longer fibrils to achieve a given degree of conversion. The other noticeable prediction of the model is a significant increase in aspect ratio at the higher temperatures of polymerization, and in this section we examine briefly whether this can be reconciled with the structural results of Section 4 where fibril misorientation was also found to increase with polymerization temperature.

Before turning to the major effect of the misorientation resulting from removal of monomer, it is worth noting that the *intrinsic* misorientation of the *c*-axis is also a maximum for the highest polymerization temperature. This accords well with the idea that aspect ratios are large under these conditions, since a long fibril is more likely to be diverted during its growth (e.g. to avoid other polymerizing regions) than one which terminates before it has grown very far.

There are two possible reasons for the fibril misorientation which occurs on removal of monomer. Firstly, if the fibrils behave as rigid rods they may simply tilt under their own weight when supporting monomer sublimes away. This is unlikely except at very low conversions, because the mechanical data reveal a surprising degree of integrity in the fibrillar specimen. The fibrils must, therefore, be firmly attached to one another as envisaged in the mechanical model of the previous section, and simple tilt could not occur. Alternatively we can imagine that the fibrils distort or bend under the influence of differential vapour pressures as the monomer sublimes or due to the relief of lattice strains. This can occur despite strong inter-fibrillar linkages and is likely to produce much greater disorientation in high aspect ratio fibrils than in short rod-like ones.

It is not easy to quantify these effects, but the following simple calculation indicates the nature of the dependence one might expect of misorientation angle ψ upon aspect ratio $2n$ and conversion β.

Elasticity theory for the bending of a square section cantilever beam gives the deflection δ produced by a force W as,

$$\delta = \frac{4W}{E}\frac{l^3}{d^4} \tag{13}$$

where $l\,(=nd)$ is the length of the fibril and E its Young's modulus. The geometrical resistance to bending is characterized, of course, by the term l^3/d^4. The mean angle of deflection, ψ is, for small angles,

$$\psi = \delta/l = Kl^2/d^4 = Kn^2/d^2 \tag{14}$$

where K is a term involving W and E.

The aspect ratio is related to the conversion by the expression

$$nd^3 = \beta/2N \tag{15}$$

where N is the number of identical fibrils in unit volume, so that

$$\psi = Kn^2\left(\frac{\beta}{2Nn}\right)^{-2/3}$$

$$\psi = \frac{Kn^{8/3}(2N)^{2/3}}{\beta^{2/3}}\,. \tag{16}$$

This equation suggests that the misorientation should have a near-hyperbolic dependence on conversion, becoming very large as $\beta \to 0$, should increase with fibril density at a given β,

and should rise sharply with increasing aspect ratio n. Whilst Fig. 2 gives no evidence on the second of these points, the first and third are amply supported by the data. It can be concluded then, that the structural results strongly support the explanations advanced to account for the mechanical data.

References

1. K. HAYASHI, H. OCHI and S. OKAMURA, *J. Polymer Sci.* **A2** (1964) 2929.
2. J. HENGSTENBERG, *Annalen Der Phsik* **84** (1927) 245.
3. E. SAUTER, *Z. Physik Chem.* **B18** (1932) 417; **B21** (1933) 186.
4. M. L. HUGGINS, *J. Chem. Phys.* **13** (1945) 37.
5. H. TADOKORO, T. YASUMOTO, S. MURAHASHI and I. NITTA, *J. Polymer Sci.* **44** (1960) 266.
6. G. A. CARAZZOLO, *ibid* **A1** (1963) 1573.
7. E. H. ANDREWS and G. E. MARTIN, *J. Mater. Sci.* **8** (1973) 1315.
8. G. A. CARAZZOLO, S. LEGHISSA and M. MAMMI, *Die Makromolek Chemie* **60** (1963) 171.
9. J. P. COLSON and D. H. RENEKER, *J. Appl. Phys.* **41** (1970) 4296.
10. D. H. RENEKER and J. P. COLSON, *ibid* **42** (1971) 4606.
11. Y. CHATANI, T. UCHIDA, H. TADOKORO, K. HAYASHI, N. MASANOBU and S. OKAMURA, *J. Macromol. Sci. (Phys)* **4** (1968) 567.
12. V. S. RYSKIN and A. I. SLUTSKER, *Poly. Sci. U.S.S.R.* **12** (1970) 2068.
13. A. MUNZO-ESCALONA, E. W. FISCHER and G. WEGNER, IVPAC Internat. Symposium (1969) p. 103.
14. D. H. RENEKER, private communication (1973).
15. I. SAKURADA, Y NUKUSHIMA and T HO, *J Polymer Sci* **57** (1962) 651; *Die Makromol Chemie* **75** (1964) 1.
16 T. MIYAZAWA, *Rep. Prog. Polymer Phys. Jap.* **8** (1965) 47.
17. A. I. SLUTSKER, A. E. GROMOV and V. S. PSHEZHETSKII, *Soviet Physics – Solid State* **6** (1964) 362.
18. I. ISHIGAKI, A. ITO, T. IWAI and K. KUBAYASHI, *J. Polymer Sci.* **A1** (1971) 2511.
19. C. W. BUNN, "Chemical Crystallography" (Oxford University Press, 1961) p. 438.

Received 4 March and accepted 25 March 1974.